ENVIRONMENTAL EPIGENETICS

Environmental Epigenetics, 2017, 1–16

doi: 10.1093/eep/dvx013
Research article

RESEARCH ARTICLE

Trichloroethylene-induced alterations in DNA methylation were enriched in polycomb protein binding sites in effector/memory CD4$^+$ T cells

Kathleen M. Gilbert[1,*], Sarah J. Blossom[1], Brad Reisfeld[2], Stephen W. Erickson[1,4], Kanan Vyas[1], Mary Maher[1], Brannon Broadfoot[1], Kirk West[1], Shasha Bai[1], Craig A. Cooney[3,‡] and Sudeepa Bhattacharyya[1,‡]

[1]Arkansas Children's Research Institute, University of Arkansas for Medical Sciences, Little Rock, AR 72202, USA, [2]Colorado State University, Fort Collins, CO 80523, USA, [3]Central Arkansas Veterans Healthcare System, Little Rock, AR 72205, USA and [4]Present address: RTI International, Research Triangle Park, NC 27709, USA

*Correspondence address. Arkansas Children's Research Institute, University of Arkansas for Medical Sciences, 13 Children's Way, Little Rock, AR 72202, USA. Tel: +1-501-364-4587; Fax: +1-501-364-2403; E-mail: gilbertkathleenm@uams.edu

‡Equally contributing authors.

Abstract

Exposure to industrial solvent and water pollutant trichloroethylene (TCE) can promote autoimmunity, and expand effector/memory (CD62L) CD4$^+$ T cells. In order to better understand etiology reduced representation bisulfite sequencing was used to study how a 40-week exposure to TCE in drinking water altered methylation of ~337 770 CpG sites across the entire genome of effector/memory CD4$^+$ T cells from MRL+/+ mice. Regardless of TCE exposure, 62% of CpG sites in autosomal chromosomes were hypomethylated (0–15% methylation), and 25% were hypermethylated (85–100% methylation). In contrast, only 6% of the CpGs on the X chromosome were hypomethylated, and 51% had mid-range methylation levels. In terms of TCE impact, TCE altered ($\geq$ 10%) the methylation of 233 CpG sites in effector/memory CD4$^+$ T cells. Approximately 31.7% of these differentially methylated sites occurred in regions known to bind one or more Polycomb group (PcG) proteins, namely Ezh2, Suz12, Mtf2 or Jarid2. In comparison, only 23.3% of CpG sites not differentially methylated by TCE were found in PcG protein binding regions. Transcriptomics revealed that TCE altered the expression of ~560 genes in the same effector/memory CD4$^+$ T cells. At least 80% of the immune genes altered by TCE had binding sites for PcG proteins flanking their transcription start site, or were regulated by other transcription factors that were in turn ordered by PcG proteins at their own transcription start site. Thus, PcG proteins, and the differential methylation of their binding sites, may represent a new mechanism by which TCE could alter the function of effector/memory CD4$^+$ T cells.

Key words: trichloroethylene; immunotoxicity; autoimmunity; DNA methylation; polycomb proteins

Received 12 May 2017; **revised** 30 June 2017; **accepted** 3 July 2017

Introduction

Approximately 24 million Americans have one or more autoimmune disease (e.g. Type I diabetes, systemic lupus erythematosus, autoimmune hepatitis). These chronic and incurable diseases disproportionately affect women, and are among the leading causes of death for young and middle-age women. In order to prevent these chronic incurable diseases we need to know more about the factors that trigger and maintain their pathology.

Effector/memory $CD4^+$ T cells that secrete IFN-γ or IL-17 are critical mediators of both idiopathic and experimental autoimmune disease [1, 2]. These $CD4^+$ T cells can persist for years in humans and animals without causing disease, while maintaining a memory phenotype, a stable cytokine response pattern, and the capacity for induced autoimmune attack [1]. Several adoptive transfer studies have shown that memory $CD4^+$ T cells that have differentiated into Th1 or Th17 cells and reactivated can provide crucial help to cytotoxic $CD8^+$ T cells, promote generation of pathogenic autoantibodies, and secrete tissue-damaging pro-inflammatory cytokines [3, 4].

Understanding how autoimmune disease triggers differentiation of naïve $CD4^+$ T cells into pro-inflammatory effector/memoryTh1 or Th17 cells is important for defining etiology. Twin concordance studies have shown that although genetics may increase susceptibility to autoimmunity, environmental triggers are required to initiate disease. Our work examining the link between the environment and $CD4^+$ T cell differentiation has focused on the volatile organic compound trichloroethylene (TCE). Although the use of TCE as a solvent in the USA has declined as its toxicity became more apparent, over 31 million pounds of TCE-containing waste was released or disposed of in this country in the last decade alone (https://www.epa.gov/toxics-release-inventory-tri-program). Because of its improper disposal over the years, TCE has contaminated many of the water systems in the USA [5].

TCE is one of the first 10 chemicals selected for risk evaluation by the EPA under the newly revised TSCA (Toxic Substances Control Act) (https://www.epa.gov/assessing-and-managing-chemicals-under-tsca/evaluating-risk-existing-chemicals-under-tsca#chemicalnames). This list was compiled based on the highest combined hazard, exposure, persistence and bioaccumulation characteristics. One of the most sensitive non-cancer outcomes of TCE exposure is immunotoxicity [6]. Specifically, chronic exposure to TCE (occupational or environmental) has been linked to a variety of autoimmune diseases and other hypersensitivity disorders [7–15].

$CD4^+$ T cells are especially susceptible to the effects of TCE. Even if overt disease is not diagnosed, increased numbers of activated $CD4^+$ T cells are often found in humans exposed to TCE [7, 16–19]. An expansion of peripheral blood $CD4^+$ T cells is also a biomarker for patients with TCE-induced hypersensitivity [20]. Finally, as shown by ourselves and others, TCE exposure increased the percentage of effector/memory IFN-γ- and Th17-secreting $CD4^+$ T cells in mice that went on to develop $CD4^+$ T cell-mediated autoimmune hepatitis [21–23].

It has recently been reported that $CD4^+$ T cell differentiation into different effector/memory $CD4^+$ T cell subsets (Th1, Th2, Th17 and T_{reg}) is at least partially regulated by gene-specific (i.e. *Ifng*, *Il17A*, *Ctla*, *Tnfsf14*, and *Foxp3*) increases or decreases in DNA methylation [24, 25]. This differentiation process can be disrupted during the development of autoimmunity, resulting in inappropriate DNA methylation and associated expression of genes that encode pro-inflammatory cytokines, chemokines, adhesion molecules, or suppressive mediators (e.g. *LTA*, *CD11α*, *CD70*, *CD40L*, *FOXP3*) [26–34]. The dysregulated methylome in autoimmune disease can enhance heterogeneity or plasticity in $CD4^+$ T cell subsets that can increase disease severity [35, 36]. For example, the most pathogenic $CD4^+$ T cells in models of type 1 diabetes mellitus, arthritis, and multiple sclerosis are those that secrete both IL-17 and IFN-γ, i.e. exhibit a dual Th1/Th17 phenotype [37]. Thus, the development of autoimmune disease may represent a breakdown in normal DNA methylation patterns in a manner that increases the differentiation of pathogenic effector/memory $CD4^+$ T cells. Demonstrating that a toxicant such as TCE can disrupt the methylome is important for understanding how toxicants promote autoimmunity.

We reported previously that a 12-week exposure to TCE in drinking water altered global methylation in effector/memory $CD4^+$ T cells from MRL+/+ mice [38]. A subsequent study, using targeted bisulfite next generation sequencing of amplicons generated on a Fluidigm Access Array, examined TCE- and time-dependent changes in DNA methylation associated with 16 functionally important genes in $CD4^+$ T cells. TCE was found to increase gene-specific methylation variance in effector/memory $CD4^+$ cells [6], and to induce a time-dependent cumulative increase in DNA methylation in the CpG sites of the promoter of the *Ifng* gene [39].

The methylome is even larger than the transcriptome. Thus, although a gene targeted evaluation of DNA methylation may provide important information about TCE-induced epigenetic alterations of specific genes, it may not recognize more global alterations in the methylome induced by TCE exposure. Consequently, the current study used reduced representation bisulfite sequencing (RRBS) [40], for a more comprehensive look at the impact of TCE exposure on CpG sites across the entire genome. A concurrent transcriptomic analysis was conducted so that TCE-induced alterations in DNA methylation could be compared with associated changes in gene expression.

Materials and Methods

Ethics Statement

All work was approved by the Animal Care and Use Committee at the University of Arkansas for Medical Sciences, and conformed to the USDA Animal Welfare Act and Regulations.

Mouse Treatment

Female MRL+/+ mice were selected for this study. Autoimmune disease in humans is known to involve an ill-defined genetic predisposition, and is most often found in women. Young adult female MRL+/+ mice, with a propensity for autoimmunity but absence of overt disease, can be used to mimic these requirements, and are used to test for the ability of different toxicants to trigger or augment autoimmunity as previously described [38]. Eight week-old female MRL+/+ mice (Jackson Laboratories; Bar Harbor, ME, USA) were housed in polycarbonate ventilated cages and provided with lab chow (Harlan 7027) and drinking water *ad libitum*. TCE (purity 99+%; Aldrich Chemical Co. Inc.; Milwaukee, WI, USA) was suspended in drinking water with 1% emulsifier Alkamuls EL-620 from Rhone-Poulenc (Cranbury, NJ). The mice (8–9 mice/group) received either 0 or 0.5 mg/ml TCE in their drinking water for 40 weeks. Freshly made TCE-containing drinking water was provided every 3–4 days. The mice were weighed once a month. On the basis of water intake, body weight and measured TCE degradation in the water bottles the

mice were exposed to an average of 40–50 mg/kg/day TCE. This does is occupationally relevant based on the current 8-h Permissible Exposure Limit [established by the Occupational Safety and Health Administration (OSHA)] for TCE is 100 ppm or ~76 mg/kg/day.

CD4$^+$ T Cells

Mice were sacrificed after 40 weeks, and splenic CD4$^+$ T cells were isolated using Dynabeads FlowComp Mouse CD4 kit (Invitrogen). The CD4$^+$ T cells were then further separated into CD62L^{lo} or CD62L^{hi} CD4$^+$ T cell populations using Dynabeads M-280 Streptavidin (Invitrogen) conjugated with biotinylated anti-CD62L antibody (eBiosciences, 13-0621-85). The resulting CD62L^{lo} CD4$^+$ T cells (effector/memory CD4$^+$ T cells) were stimulated with immobilized anti-CD3 antibody and anti-CD28 antibody for 18 has described [41], and the activated CD4$^+$ T cells were frozen for subsequent examination of DNA methylation or transcriptomics. To ensure sufficient cells for use in all the assays each sample of CD4$^+$ T cells used in the study originated in an equal number of pooled spleen cells from 2 to 3 mice resulting in four samples/treatment group.

DNA Methylation Analysis by RRBS

DNA from the CD4$^+$ T cells (four control samples and four TCE samples) was isolated using the PureLink Genomic DNA Mini Kit (Thermo Fisher Scientific). The resulting DNA is tested on the NanoDrop 2000c (Thermo Fisher Scientific) for an A260/A280 range of 1.8–2.0. DNA quality is then confirmed using standard gel electrophoresis. The DNA was then restriction digested, end-repaired, purified, and attached with barcode adapters [42]. The RRBS libraries were generated, bisulfite converted, PCR enriched, size selected, purified, and sequenced (2×100 paired end) using an Illumina HiSeq sequencer (UAMS Translational Research Institute Genomics Core).

The Fasta files containing sequenced reads were first quality checked using FastQC program v0.11.5 and trimmed for adapter and low-quality sequences using trim galore (http://www.bioinformatics.babraham.ac.uk/projects/trim_galore/) with a Phred score of 20 as cut-off. Sequences were mapped using paired end mapping to mouse genome assembly mm9 using Bismark software v0.16.1 with Bowtie 2 v2.2.8 short read aligner. In the final step of bismark_methylation_extractor module, C in CpG, CHH and CHG were extracted with the parameter—no_overlap, to ensure that overlapping reads from the paired reads were not measured twice in the final analysis. Additionally, due to detection of consistently higher methylation rate at the ends of the sequencing reads in M-bias plots (data not shown), three bases from the ends of each pair of reads were discounted for methylation extraction. Bismark's methylation_extracter output files were then read into MethylKit R package [43] for further statistical analyses.

Differential Methylation Analysis

A Phred Quality Score (Q) is used to represent the confidence level in assignment of each base call by the sequencer. It is logarithmically related to error probability and gives an estimated probability of a base call being wrong. In bisulfite sequencing a Phred score of 20 is normally used as a cut-off, and is the default value used in many open source sequencing tools [44]. Similarly, 10 reads is the minimum number of reads required for accurate determination of DNA methylation if individual CpG sites are analyzed for methylation differences [45]. Consequently, only sequence reads with a Phred score >20 and a minimum of 10 reads per CpG were accepted for downstream statistical analysis. Reads above the 99.9 percentile were also filtered out since these reads are either mapped against repeat elements or have very high PCR bias. A logistic regression model was fitted per CpG site to test for TCE effect on methylation level using a FDR cut off of 5% and a methylation difference of at least 10%.

In order to test the difference between TCE and control mice in terms of the relationship between mean methylation variance and mean percent methylation, quadratic regression models including the quadratic and linear interaction between groups and average percent methylation were fit to the data. A likelihood ratio test was used to compare the TCE and control curves by fitting and comparing a full model and a reduced model. The full model includes quadratic and linear interaction between groups (TCE vs control) and average percent methylation, while the reduced model includes common quadratic and linear terms of average percent methylation for both TCE and control.

qRT-PCR

Fluorescence-based quantitative reverse transcriptase polymerase chain reaction (qRT-PCR) was conducted using RNA isolated from effector/memory CD4$^+$ T cells using techniques and primers as described [21]. Fold differences ($\log_2$ scale) in expression were determined using expression levels of resting (unactivated) CD4$^+$ T cells of the appropriate subset of control mice as the control (1×) expression level. The threshold for statistical significance in fold change was set at $P < 0.05$. Differences between experimental groups were tested first with analysis of variance (ANOVA), and where the F test was significant, subsequent pairwise contrasts were tested using a two-sample t-test. CD4$^+$ T cell concentration and gene expression values were right-skewed, and therefore these data were log-transformed for statistical analyzes. Adjusting for multiple comparisons, P-values from pairwise comparisons that were smaller than the Bonferroni-adjusted significance level indicated statistical significance.

Gene Arrays

This assessment was conducted by the Genomics Core at the University of Arkansas for Medical Sciences. All RNA samples extracted from CD4$^+$ T cells had RIN (RNA integrity number) values of 8.0 or above. Total RNA (500 ng) was converted to cDNA, amplified and biotinylated by use of the Ambion Illumina TotalPrep^{TM}-96RNA Amplification Kit (Life Technologies, Carlsbad, CA, USA). Gene expression profiling was performed using the Expression BeadChip System from Illumina (Illumina Inc., San Diego, CA, USA) following the manufacturer's instructions. Raw data were $\log_2$ transformed and normalized to the median intensity signal of 47 231 genes on the array. After normalization and filtering of low intensity spots, two-sample Student's t-tests were performed and these data were plotted against fold-change measurements. Statistical significance was set at false discovery rate (FDR) < 0.05. Ingenuity Pathway Analysis software (Redwood City, CA, USA) was used for network identification.

Modeling

Fractional Polynomials were fit to model the percentage of total CpG sites that displayed a particular level of mean methylation

(e.g. CpG sites that averaged 0–5% methylation or 40–45% methylation). This model has more flexibility to obtain a wide range of shapes of the distribution of the data than regular polynomial models. The power of mean methylation binning were chosen among {-2, -1, -0.5, 0, 0.5, 1, 2, 3} and were allowed to be repeated. The best-fitting first-degree FP model was the one with the lowest deviance among all first-degree powers. The best-fitting second-degree FP model was determined the same way after searching through all possible second-degree power combinations. The final best-fitting model was decided among the four models: null, linear, best-fitting first-degree FP, and best-fitting second-degree FP using a close testing procedure [46]. The final sets of powers selected for the best-fitting model for each chromosome in control or TCE groups were then compared. Having the same set of power suggests that the distribution is similar while a different set of powers suggests the distribution is different.

Annotation of the CpGs and Regulatory Elements was done using the University of California, Santa Cruz, Genome Browser (mouse NCBI37/mm9).

Results

Large-Scale Effects of TCE on DNA Methylation in Effector/Memory CD4$^+$ T Cells

RRBS analysis of the effector/memory CD4$^+$ T cells collected after 40 weeks of adult exposure to TCE was conducted. The analysis incorporated ~337 770 CpGs sites that were assayed with at least 10× coverage. Bisulfite conversion efficiency in all samples was > 99%. Figure 1A presents histograms showing the average methylation of all the CpG sites examined after binning for average methylation (e.g. 0–5% methylation or 20–25% methylation). These profiles demonstrated that 54.7% and 16.5% of CpG sites from control mice were hypomethylated (0–5% methylation) or hypermethylated (95–100% methylation), respectively. These values were slightly altered in CD4$^+$ T cells from TCE-treated mice; with 54.2% hypomethylated and 15.9% hypermethylated CpG sites respectively. Representing the binned mean methylation results without the hyper- and hypo-methylation skewing the extreme ends of the histogram (Fig. 1B) illustrated TCE-induced differences in the percentage of CpGs methylated at 90–95% (4.9% vs 6.0%; $P < 0.05$).

The average methylation levels of CpGs on individual chromosomes were also examined. With the exception of the X chromosome, most of the chromosomes showed very similar methylation profiles (Fig. 2A). In other words, most had similar percentages of CpGs with hypo-, hyper- and mid-range methylation levels, regardless of whether they came from CD4$^+$ T cells from control or TCE-treated mice. Unlike the 19 autosomal chromosomes, very few (~2.4%) of the CpGs interrogated in the X chromosome displayed methylation levels between 0 and 5%. Instead, the X chromosome had a slightly higher percentage (18.3%) of CpGs with mean methylation levels between 95 and 100%, and a considerably higher percentage (51%) of CpGs with mean methylation levels between 15 and 60%, peaking around 40% mean methylation. This effect was more visually striking after removing from the histograms all CpGs with 0–5% or 95–100% methylation (Fig. 2B). The difference in the average methylation histogram of the X chromosome was confirmed by Fractional Polynomial modeling (Supplementary Table S1 and Supplementary Fig. S1). This modeling showed that the basic shape of the methylation distribution did not differ among representative autosomal chromosomes (chromosomes 1, 3 or 12),

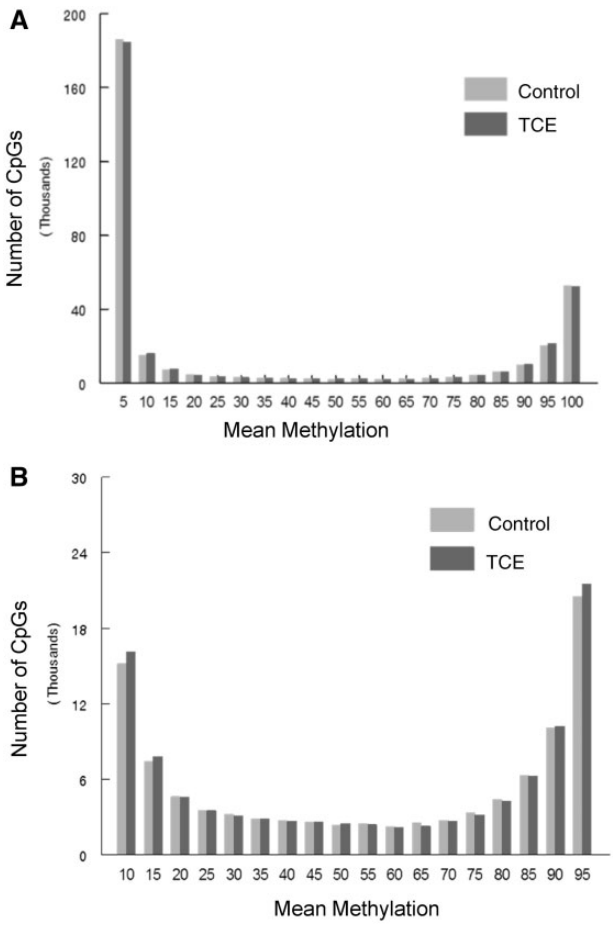

Figure 1: Average DNA methylation levels of all CpGs interrogated. RRBS analysis of the effector/memory CD4$^+$ T cells collected after 40 weeks of adult exposure to TCE was conducted. (**A**) Histograms show the average methylation of all 337 770 CpG sites examined in CD4$^+$ T cells from either control or TCE-treated mice after binning for average methylation (e.g. 0–5% methylation or 20–25% methylation). (**B**) The same histograms are shown without inclusion of the CpGs that were either 0–5% or 95–100% methylated

regardless of TCE exposure, but that all are different from the X chromosome. Figure 2B also reveals other apparent chromosome-specific differences in the shape of the methylation distribution histograms. For example, chromosome 17 has increased mid-range DNA methylation levels, while several other chromosomes (e.g. 16, 18 and 19) had flattened U-shape histograms indicated less skewing toward hypo- or hypermethylation status. The chromosome-specific differences in CpG mean methylation appeared to be inherent, i.e. were not induced by TCE exposure.

When the mean methylation of thousands of CpG sites was examined, as shown in Figs 1 and 2, no TCE-induced effect was detected. However, global effects on DNA methylation can also occur at the level of methylation variance [47]. Methylation variance reflects the group-specific inter-sample variation in the methylation of each CpG site, rather than mean methylation of each CpG site. An examination of all the CpGs interrogated showed that mean methylation variance detected in effector/memory CD4$^+$ T cells, regardless of TCE treatment, was substantially lower than the theoretical variance that would be achieved by random distribution in a percent mean methylation bin (Fig. 3). However, as we and others have previously reported, inter-sample methylation variance at the CpG sites examined

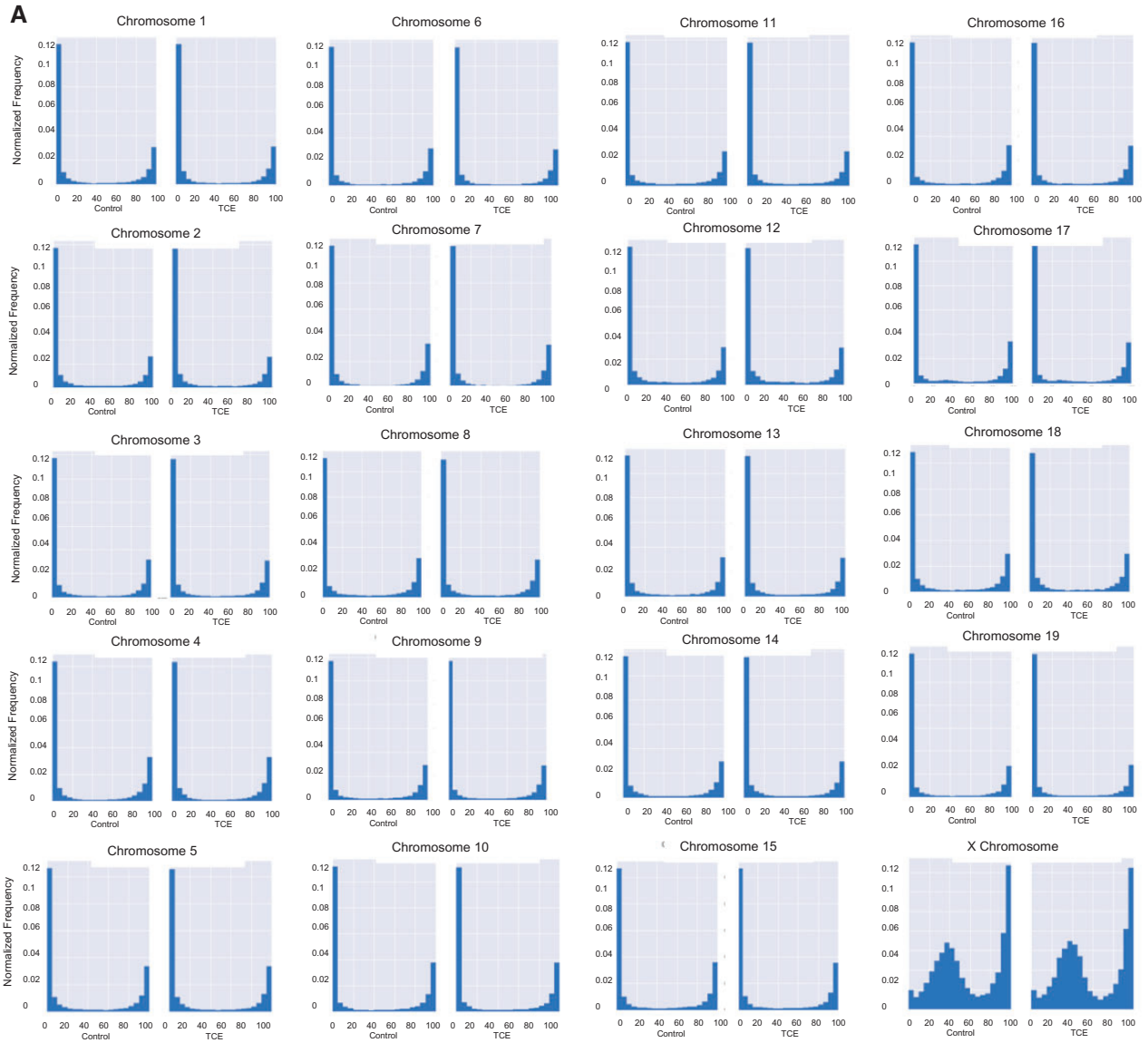

Figure 2: Chromosome-specific mean DNA methylation levels. (**A**) The results from the RRBS analysis described in Fig. 1 were sorted into individual chromosomes, and presented after binning for average methylation of the CpGs. The area of each histogram was normalized to one to make it easier to compare the chromosomes. (**B**) The RRBS results were presented (as total number of CpG sites in the different bins) after excluding the CpG sites that were either 0–5% or 95–100% methylated

in effector/memory CD4$^+$ T cells correlated with distance to either end of the 0–100% methylation scale [6, 48]. Thus, mean methylation variance in both control and TCE samples was highest at those CpG sites that averaged 30–80% methylation (Fig. 3). Interestingly, exposure to TCE decreased the methylation variance at CpGs at almost all levels of mean methylation. This was true for the X chromosome as well, despite its different mean methylation distribution (data not shown). A likelihood test statistic of 75.8 (*P*-value < 0.0001) suggested that the curves documenting methylation variance for all the CpGs interrogated (Fig. 3) are significantly different between the samples from control and TCE-treated mice. We evaluated the methylation variance for each of the CpG sites that averaged between 50 and 60% methylation for four individual control samples (Supplementary Fig. S2). This revealed that the variance in the control group could not be attributed to an outlier sample, but appeared to represent a consistent difference among all the samples. Thus, the ability of TCE to impact CpG methylation on a genome-scale, as evidenced by this decrease in methylation variance, did not appear to be artefactual.

Effects of TCE at the Individual CpG Level

In addition to assessing the genome-scale effects of TCE on DNA methylation, individual CpG sites that were differentially methylated by TCE exposure were identified. Comparison of effector/memory CD4$^+$ T cells from control and TCE-treated mice revealed 233 differentially methylated sites (DMS, q value $<$ 0.005, and methylation differences $\geq$ 10%). Hierarchical clustering of the DMS is shown in Fig. 4A. Annotation of the DMS indicated that the 233 DMS were associated with 216 genes after taking into account those instances in which two or more CpGs were associated with the same gene. Further evaluation for potential functional significance narrowed down the list to 157 DMS that were actually located in a gene, or within 5 kb upstream of the transcription start site (TSS), and thus in a

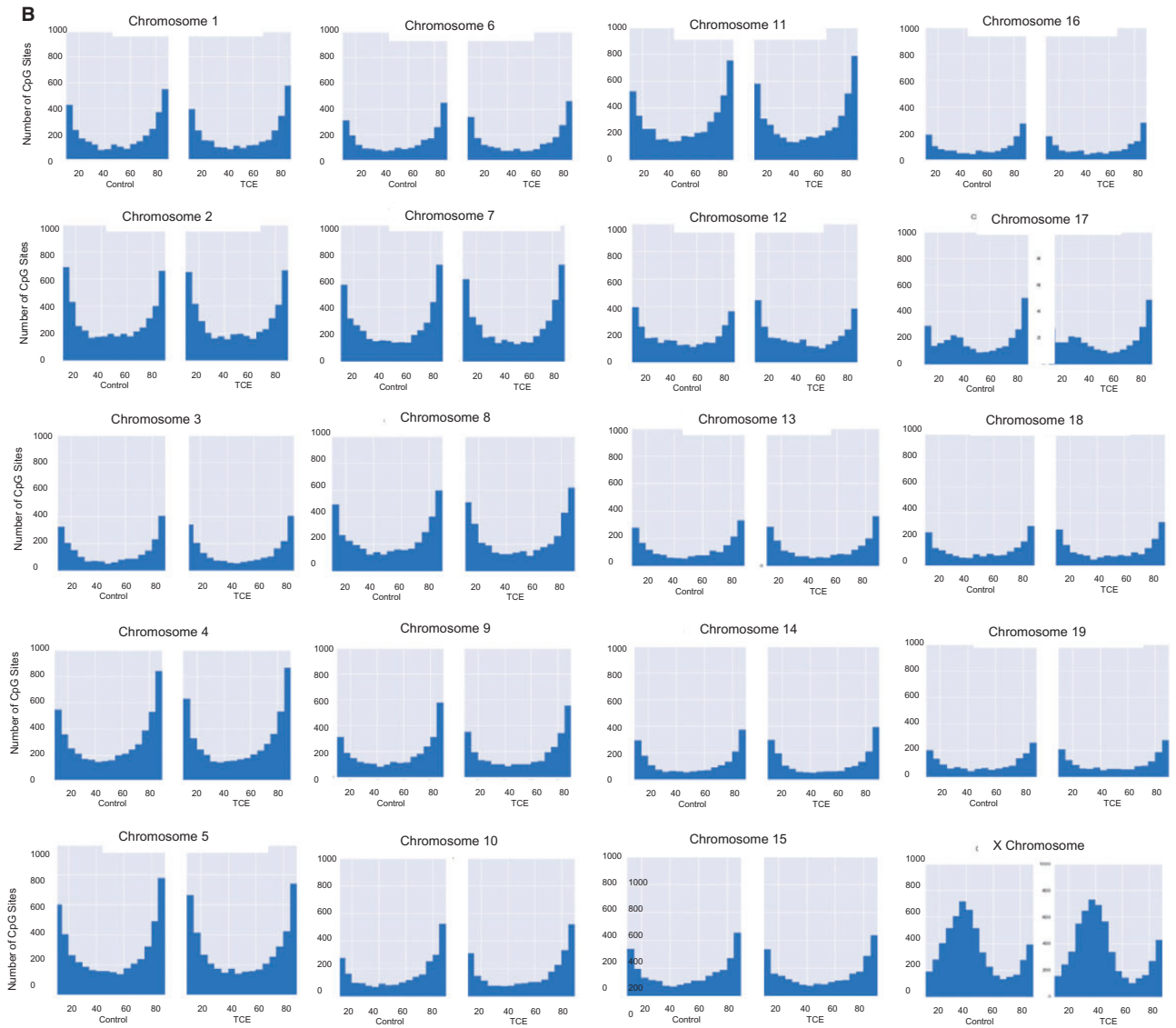

Figure 2: Continued

possible promoter region. As shown in Fig. 4B, more DMS were found downstream compared with upstream of the TSS. Distribution from TSS was not normally distributed (*P*-value of Shapiro–Wilk tests is <0.001, rejects the null hypothesis which is data are normally distributed). Examination of symmetry plot and quantile–quantile plot shows that the data are heavy-tailed. The greatest number of DMS were located within 5 kB downstream of the TSS. Thus, TCE tended to alter methylation of CpG sites in the gene body close to the TSS more often than it altered sites in a traditional promoter region.

Pathway analysis of the CpG sites differentially methylated by TCE indicated that, in terms of molecular function, TCE primarily altered methylation of genes associated with binding (GO:0005488) (Fig. 4C). Drilling down in the binding molecular function category showed that TCE effects were focused on genes associated with nucleic acid binding (GO:003676), that were in turn enriched for genes associated with DNA binding (GO:0003677). TCE also differentially methylated genes associated with protein binding (GO:0005515), specifically transcription factor binding activity (GO:0000988). Taken together, TCE

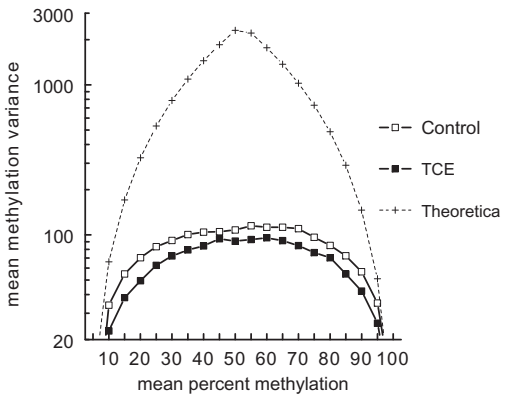

Figure 3: TCE exposure decreased total methylation variance. The RRBS results for the effector/memory $CD4^+$ T cells from control or TCE-treated mice were sorted by treatment group and binned for mean methylation. The inter-sample methylation variance at all the CpG sites in the different bins was then calculated. The dotted line represents a prediction of highest possible methylation variance based on a theoretical value spread of four samples in each bin

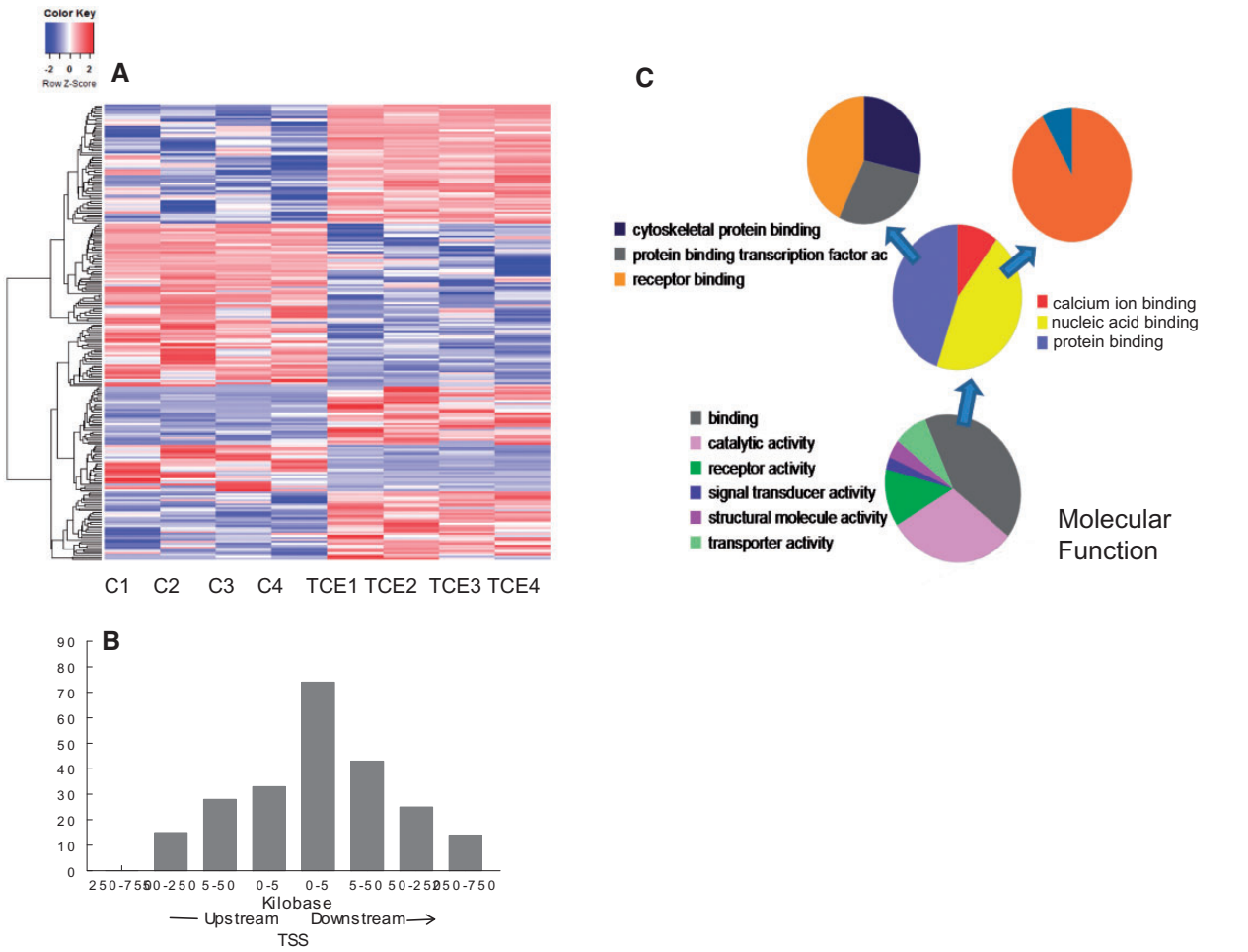

Figure 4: Identification of CpG sites differentially methylated by TCE exposure. (**A**) RRBS analysis of effector/memory CD4$^+$ T cells from control and TCE-treated mice revealed 233 DMS (methylation difference $\geq$ 10%, q value $<$0.005). Hierarchical clustering of the gene-associated DMS is shown here. (**B**) The genomic location of the 233 DMS detected in the effector/memory CD4$^+$ T cells relative to the nearest transcription start site (TSS) is shown. (**C**) The genes associated with the DMS identified by the RRBS were subjected to a gene list functional analysis by the Panther Gene Ontology Classification System

exposure altered DNA methylation in a manner that seemed primed to impact epigenetic function and gene expression.

When the CpG sites that were differentially methylated between control and TCE samples were binned by average percent methylation in effector/memory CD4$^+$ T cells from control mice the profile included many CpG sites with mid-range methylation (Fig. 5). The percentage of DMS with hypo-methylated (0–20%) and hyper-methylated (80–100%) status was much lower than those found in the evaluation of all the CpGs interrogated (as shown in Fig. 2). When the differentially methylated CpG sites were binned by average percent methylation in effector/memory CD4$^+$ T cells from TCE-treated mice, it showed that, compared with controls, TCE decreased the number of CpG sites with 60–80% methylation, and increased the number of CpG sites that averaged 80–100% methylation. This suggested that the effect of TCE on DNA methylation was skewed toward inducing hyper- rather than hypo-methylation.

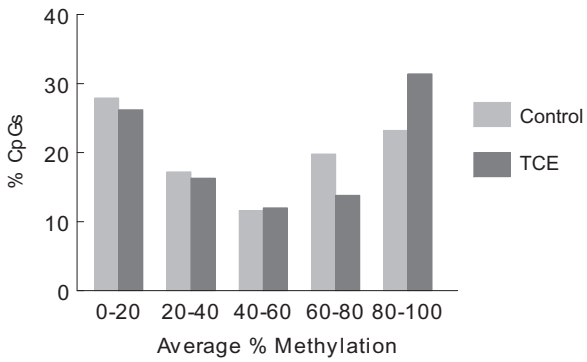

Figure 5: Average percent methylation of CpG sites differentially methylated by TCE. RRBS analysis of effector/memory CD4$^+$ T cells from control and TCE-treated mice revealed 233 DMS (methylation difference $\geq$ 10%, q value $<$ 0.005). These DMS were sorted separately for control and TCE-treated samples and binned for mean methylation

Enrichment for Polycomb Protein Binding Sites

A single CpG may indicate the DNA methylation status of the surrounding region in which differential methylation of other individual sites may not reach the level of statistical significance. Thus, alterations in methylation of single CpGs in regulatory regions can have potential functional importance. The Mouse NCB137/mm9 genome in the UCSC Genome Browser was used to determine whether the DMS were located in regulatory elements that bound transcription factors, and thus might impact transcription. Of the 233 DMS, 87 (37.3%) were found in

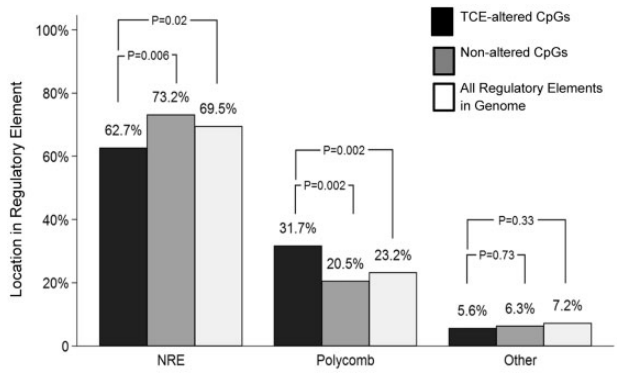

Figure 6: Many CpG sites differentially methylated by TCE are found in PcG protein binding sites. RRBS analysis of effector/memory CD4$^+$ T cells from control and TCE-treated mice revealed 233 DMS (methylation difference $\geq$ 10%, q value $<$ 0.005). Annotation of these DMS described whether they were found outside of a transcription binding site (NRE: no regulatory element), or in a regulatory element that bound PcG proteins or other transcription factors. The percentage of CpG sites differentially methylated by TCE was compared with 400 randomly selected CpG sites not altered by TCE (Random CpGs), and to the total number of individual OREG sites known to bind Suz12, EZH2, Mtf2 or Jarid2 or other transcription factors (as identified in Mouse NCB137/mm9 genome in the UCSC Genome Browser) (All Regulatory Elements in Genome)

regulatory elements with annotated transcription factor binding sites. Analysis of these 87 DMS revealed that 85% were found in regions exclusively used to bind one or more of four different Polycomb group (PcG) proteins, namely Ezh2, Suz12, Mtf2 or Jarid2 (Fig. 6; Table 1). The remaining 15% DMS in regulatory regions were found in binding sites for other transcription factors (e.g. Ebf1, Gata1, Nfe212, and ATOH). This distribution was somewhat surprising since only ~19 000 (4.5%) or the ~399 000 unique transcription factor binding sites in the whole mouse genome are thought to bind one or more PcG protein. The TCE-induced modifications of CpG sites in the PcG protein binding regions were evenly divided between increased and decreased methylation. Of the DMS in polycomb binding sites, most (85%) flanked a TSS. In comparison, none of the DMS in binding sites for other transcription factors occurred in a region that flanked a TSS. Indeed, an evaluation of all 337 770 CpGs sites interrogated in the effector/memory CD4$^+$ T cells revealed that only 23.2% were found in PcG protein binding regions, while only 7.2% were found in regulatory regions targeted by other transcription factors. Thus, our evaluation of effector/memory CD4$^+$ T cells suggests that PcG protein binding regions are enriched for CpG sites. It is possible that the CpG sites in these regions of effector/memory CD4$^+$ T cells may be particularly sensitive to TCE-induced alterations.

TCE Alters CD4$^+$ T-Cell Gene Expression

The functional effects of TCE exposure were further assessed at the gene expression level. This was accomplished using a microarray assessment of the same cells as those profiled in the RRBS analysis: i.e. effector/memory (CD62L^{lo}) CD4$^+$ T cells collected from control mice or from mice exposed to TCE for 40 weeks. Gene expression was examined 20 h after activation of the CD4$^+$ T cells *in vitro*. At a cutoff of FDR $<$ 0.05 and a fold-change $>$ 1.25, the expression of ~560 genes was found to be significantly altered in the activated effector/memory CD4$^+$ T cells of mice exposed to TCE compared with similarly activated effector/memory CD4$^+$ T cells from control mice (data not shown). Of these differentially expressed genes, those associated with immune function are listed in Table 2. A network evaluation suggested that pathways with the most number of genes altered by TCE after 40 weeks were those with decreases in gene expression that centered on *Ifng* and *Tnf* (Supplementary Fig. S3A). qRT-PCR analysis confirmed the TCE-induced decrease in the expression of *Ifng* and *Tnf* in the effector/memory CD4$^+$ T cells (Supplementary Fig. S3B). Of the genes altered by TCE in the effector/memory CD4$^+$ T cells, none contained the previously described DMS.

Although TCE-induced gene changes and DMS did not coincide they did share some common features. Evaluation of the first intron and 5 kb region upstream of the TSS for the immune genes altered by TCE (Table 2) showed that 10.2% had binding sites for PcG proteins, while an additional 69.4% had binding sites for other transcription factors that were in turn regulated by PcG proteins at their own TSS. This suggests that at least 80% of the genes altered by TCE in the effector/memory CD4$^+$ T cells had the potential for PcG protein regulation.

Discussion

Our RRBS evaluation of CpG methylation distributions in autosomal chromosomes in effector/memory CD4$^+$ T cells conformed to the general trend: hypomethylation $>$ hypermethylation $>$ mid-range methylation. On a genome-scale TCE appeared to decrease methylation variance of CpG sites that averaged $<$95%, or $>$5% methylation. Increased methylation variance at CpG sites that average between 30 and 60% methylation is thought to be important for maintaining flexibility in the methylation and associated expression of functionally important genes [47]. Such regions may be protected from suppressed, fully methylated states or permissive, unmethylated states. When we examined all the CpGs interrogated by RRBS in the effector/memory CD4$^+$ T cells from control mice, the variance was highest for CpGs with intermediate methylation levels. This has been described previously [6] and is related to the fact that percentage scales tend to restrict variability near the edges of the scale. In the current study, we found that TCE exposure decreased variance in CpG sites with intermediate methylation levels. The ability of TCE to impact intermediate methylation may have more functional significance than effects at the ends of the methylation scale; increasing DNA methylation from 5 to 20%, or decreasing methylation from 95 to 80% is less likely to alter gene expression.

Using a methylation difference of 10% between the two groups as the cutoff, only 233 CpGs (216 genes) of the 337 770 CpGs interrogated in effector/memory CD4$^+$ T cells were differentially methylated by TCE exposure. The relatively small TCE affect (0.07% of the CpGs examined) compares to the 0.83% of total CpGs that were found to be differentially methylated when naïve CD4$^+$ T cells were contrasted to memory CD4$^+$ T cells in humans [24]. It is perhaps not surprising that two populations of effector/memory CD4$^+$ R cells that differed only in relatively low level adult exposure to a toxicant would demonstrate less epigenetic modifications than that which accompanies CD4$^+$ T cell differentiation. A transcriptomic analysis of the same effector/memory CD4$^+$ T cells used to generate the RRBS data identified a number of immune-associated changes following TCE exposure. However, none of the differentially expressed genes overlapped with DMS in the CD4$^+$ T cells from the TCE-treated mice despite the fact that many of the DMS were found in gene bodies within 5 kb downstream of the TSS. Although cytosine methylation of promoters is negatively correlated with gene expression, the question of whether methylation of a particular

Table 1: DMS found in genes or gene promoter regions (q value < 0.005 and differential methylation $\geq 10\%$)

Chr	Position	Difference between TCE and control methylation	Refseq ID	Feature name	PcG	Other TF with PcG
chr1	52733087	19.80	NM_133829	Mfsd6	None	None
chr1	72871428	10.11	NM_008342	Igfbp2	None	None
chr1	84692366	–12.74	NM_152915	Dner	Mtf2	
chr1	87915123	12.38	NM_027029	Spata3	Mtf2, Suz12, EZH2, Jarid2	
chr1	87915176	10.91	NM_027029	Spata3	Mtf2, Suz12, EZH2, Jarid2	
chr1	88566769	–11.67	NM_010933	Nppc	Suz12, EZH2, Jarid2	
chr1	95079010	21.05	NM_001310428	Crocc2	None	None
chr10	57695435	19.10	NM_001081954	Dux	Mtf2	
chr10	59348501	38.10	NM_019965	Dnajb12	None	Ebf1
chr10	70622501	12.01	NM_031397	Bicc1	Mtf2, Suz12, EZH2, Jarid2	
chr10	80297554	26.59	NM_001013758	Lingo3	Mtf2, Suz12, EZH2	
chr10	80306503	13.08	NM_001013758	Lingo3	Mtf2, Suz12, EZH2	
chr10	114239413	–17.84	NM_146241	POL2	Mtf2, Suz12, EZH2, Jarid2	
chr10	126954849	24.03	NM_001098789	Shmt2	None	
chr10	126962175	–15.64	NM_028230	Nxph4	Mtf2, Suz12	
chr10	127733967	–12.19	NM_031252	Il23a	None	
chr11	8496658	22.56	NM_001083587	Tns3	None	None
chr11	50416921	–11.01	NM_175643	Adamts2	Mtf2, Suz12, EZH2, Jarid2	
chr11	53271010	–23.32	NM_027917	Schroom1	Mtf2, Suz12	
chr11	61267631	27.93	NM_009548	Rnf112	None	None
chr11	92958940	–13.88	NM_028296	Car 10	Mtf2, Suz12	
chr11	95692072	29.58	NM_025659	Abi3	Mtf2, Suz12, EZH2	
chr11	103222902	10.07	NM_001205236	h3d20	None	
chr11	113664146	–20.41	NM_172800	Sdk2	None	
chr11	117829957	–13.33	NM_007707	Socs3	None	
chr11	121691565	22.39	NM_029049	Ptchd3	Mtf2, Suz12	
chr12	25366541	16.22	NM_001004455	Cys1	Mtf2, EZH2	
chr12	28026694	18.76	NM_009234	Sox11	Mtf2, Suz12, EZH2	
chr12	51749480	14.75	NM_008858	Prdk1	Mtf2, Jarid2	
chr12	51749594	22.12	NM_008858	Prdk1	Mtf2, Jarid2	
chr12	77506059	13.22	NM_008301	Hspa2	Mtf2, Jarid2, EZH2, Jarid2	
chr12	81071379	17.08	NM_001252562	Rad51b	None	Ebf1
chr12	81216463	–18.69	NM_007564	Zfp36l1	Mtf2	
chr12	81794135	20.44	NM_001177503	Plekhd1	Mtf2, Suz12	
chr12	84828460	27.36	NM_001267625	Dpf3	Mtf2, Jarid2, EZH2, Jarid2	
chr12	84828462	32.76	NM_001267625	Dpf3	Mtf2, Jarid2, EZH2,Suz12	
chr12	85758595	20.16	NM_025525	Bbof1	None	None
chr12	86630006	–21.49	NM_172414	Zc2hc1c	None	None
chr12	111468610	28.44	NM_012023	Ppp2r5c	None	None
chr13	49168362	–23.74	NM_001290313	Wnk2	None	None
chr13	53560005	–23.88	NM_013601	Msx2	Mtf2	
chr13	55097204	–16.10	NM_001206390	Unca5	None	None
chr13	69137738	17.13	NM_153534	Adcy2	EZH2, Mtf2	
chr13	104899736	–10.66	NM_029447	N1n	None	None
chr13	110249606	–21.25	NM_011056	Pde4d	None	None
chr14	55195182	–22.04	NM_010590	Ajuba	None	None
chr14	64478548	–26.58	NM_028228	Pinx1	None	None
chr15	7763733	–10.39	NM_001301333	Gdnf	Mtf2, Jarid2, EZH2, Suz12	
chr15	39751326	26.27	NM_172814	Lrp12	None	None
chr15	78548459	–21.71	NM_183141	Elfn2	Mtf2, Jarid2, EZH2, Suz12	
chr15	78873745	–10.38	NM_015738	Galr3	Suz12, EZH2	
chr15	79920093	22.09	NM_009303	Syngr1	None	None
chr15	91729910	11.19	NM_198927	Muc19	None	None
chr15	101858889	–20.17	NM_010664	Krt18	Mtf2	
chr15	22440834	24.56	NM_023794	Etv5	None	None
chr16	65815534	17.40	NM_028572	Vg113	None	ATOH1
chr16	72682095	11.64	NM_019413	Robo1	None	None
chr16	84989074	13.29	NM_001198823	App	None	None
chr17	11806358	26.52	NM_016694	Park2	None	None

continued

Table 1: Continued

Chr	Position	Difference between TCE and control methylation	Refseq ID	Feature name	PcG	Other TF with PcG
chr17	26204880	–17.06	NM_001162868	Rab11fip3	Mtf1	
chr17	27787774	30.42	NM_001286743	Pascin1	None	None
chr17	32326330	14.78	NM_001033163	Ephx3	Mtf2	
chr17	35033560	20.63	NM_001286575	Zbtb12	None	None
chr17	47809520	26.89	NM_198421	Usp49	None	None
chr17	80112667	10.22	NM_009994	Cyb1b1	Mtf2, Jarid2, EZH2, Suz12	
chr17	86014548	20.07	NM_198421	SIX30S1	Mtf2, Jarid2, EZH2, Suz12	
chr18	7170227	–15.42	NM_001081393	Armc4	None	None
chr18	11997673	11.79	NM_001146287	Cables1	Mtf2, Jarid2, EZH2, Suz12	
chr18	37926514	26.30	NM_033595	Pcdhga12	Suz12	
chr18	46372273	–16.68	NM_178872	Trim36	Suz12, Mtf2	
chr18	74603497	–26.02	NM_201600	Myo5b	EZH2, Mtf2	
chr18	75980831	–36.51	NM_145356	Zbtb7c	Mtf2, Jarid2, EZH2, Suz12	
chr19	5332047	–28.01	NM_139301	Catsper1	None	None
chr19	47388615	22.47	NM_008018	Sh3pxd2a	None	None
chr19	47388661	24.44	NM_008018	Sh3pxd2a	None	None
chr2	5636284	11.52	NM_177343	Camkid	None	None
chr2	37649110	20.86	NM_001163566	Crb2	Mtf2, Jarid2, EZH2, Suz12	
chr2	37649121	20.12	NM_001163566	Crb2	Mtf2, Jarid2, EZH2, Suz12	
chr2	76176253	15.65	NM_001081033	Pdella	Mtf2	
chr2	91316809	–23.84	NM_172668	Lrp4	None	None
chr2	91475664	16.00	NM_010168	F2	None	None
chr2	126379285	–22.21	NM_011978	Slc27a2	None	None
chr2	147874612	–14.49	NM_010446	Foxa2	Mtf2, Jarid2, EZH2, Suz12	
chr2	165242677	16.72	NM_054055	Slc13a3	None	None
chr3	69120629	–12.04	NM_178726	Ppm11	Mtf2, Jarid2, EZH2, Suz12	
chr3	89229249	12.43	NM_001113331	Shc1	None	None
chr3	128906125	15.67	NM_011098	Pitx2	Mtf2, Jarid2, EZH2, Suz12	
chr3	151928358	–26.03	NM_199465	Nexn	Mtf2, Jarid2, EZH2, Suz12	
chr4	46728412	–11.11	NM_001081141	Gabbr2	None	None
chr4	65065259	–33.06	NM_019514	Astn2	None	None
chr4	80557862	10.89	NM_026821	Lurap11	None	None
chr4	117928909	15.15	NM_011213	Ptprf	None	None
chr4	124682634	–26.36	NM_138683	Rspo1	None	None
chr4	133430503	–18.16	NM_001285506	Rps6ka1	None	None
chr4	134711341	26.82	NM_019732	Runx3	Suz12	
chr4	134711350	23.31	NM_019732	Runx3	Suz12	
chr4	139379960	–22.47	NM_011039	Pax7	Mtf2, Jarid2, EZH2, Suz12	
chr4	141640595	–21.15	NM_145402	GM10565	None	None
chr4	148423617	29.44	NM_019781	Pex14	None	None
chr4	149745860	17.35	NM_001085492	Rere	None	None
chr4	151089350	26.29	NM_001081557	Camta1	None	None
chr4	152834168	18.58	NM_001099299	Ajap1	None	None
chr5	34066416	11.04	NM_001163217	Fgfr3	Mtf2, Jarid2, EZH2, Suz12	
chr5	37187480	10.53	NM_026242	Mrfap1	None	None
chr5	114723943	–11.11	NM_148935	Foxn4	None	None
chr5	122278672	22.15	NM_001306126	Sh2b3	Mtf2	
chr5	131782939	–23.02	NM_145218	Wbscr17	Mtf2, Jarid2, EZH2, Suz12	
chr5	140447989	17.64	NM_175522	Rlfn1	None	None
chr5	148138165	–13.33	NM_001039678	Urad	None	None
chr6	23210525	–18.28	NM_028462	Cadps2	Mtf2	
chr6	63207478	17.79	NM_008167	Grid2	Mtf2, Jarid2, EZH2, Suz12	
chr6	83135914	–26.38	NM_007835	Dctn1	None	None
chr6	85324297	–10.98	NM_001003955	Rab11fip5	None	None
chr6	98926364	30.44	NM_001197322	Foxp1	None	None
chr6	113342775	33.59	NM_133923	Tt113	None	None
chr6	125262312	–21.28	NM_010736	Tltpr	Mtf2	
chr7	13628786	–15.20	NM_145819	Mzf1	Suz12, Mtf2	
chr7	16726237	–11.83	NM_148946	Slc8a2	None	None

continued

Table 1: Continued

Chr	Position	Difference between TCE and control methylation	Refseq ID	Feature name	PcG	Other TF with PcG
chr7	24096775	–16.75	NM_001004194	Nirpfe	None	None
chr7	29606786	–24.74	NM_016772	Hnrnpl	None	Ebf1
chr7	35015176	13.38	NM_008155	Gpi1	None	None
chr7	52940127	18.03	NM_001289693	Sec1/Ntn5	None	None
chr7	63520836	–24.05	NM_021879	Oca2	None	None
chr7	87481393	–12.53	NM_133952	Unc45a	None	None
chr7	93301399	28.53	NM_001102578	Vmn2r75	None	None
chr7	104376316	21.11	NM_001177412	Gab2	None	None
chr7	133957534	27.42	NM_026884	Fam57b	None	ATOH1
chr7	138078229	–22.20	NM_019564	Htra1	Mtf2, EZH2, Suz12	
chr8	12430585	–10.48	NM_009233	GM5607	Mtf2	
chr8	72406588	18.95	NM_026818	Cilp2	Mtf2, Jarid2, EZH2, Suz12	
chr8	72898699	14.06	NM_016685	Comp	Mtf2, EZH2, Suz12	
chr8	73296263	–11.49	NM_008841	Pik3r2	None	None
chr8	83263159	–24.64	NM_053124	Smarca5	None	None
chr8	94882246	–12.94	NM_018826	Irx5	Mtf2, EZH2, Suz12	
chr8	107880886	–12.28	NM_001081332	Slc9a5	None	None
chr8	116729816	13.57	NM_173016	Vat1l	Mtf2, Suz12	
chr8	121971793	–19.02	NM_054095	Necab2	Jarid2, EZH2, Suz12	
chr8	125088900	26.17	NM_026014	Cdt1	None	Ebf1
chr8	125389116	–36.05	NM_007662	Cadherin 15	None	Ebf1
chr8	125389194	–30.65	NM_007662	Cadherin 15	None	Ebf1
chr8	125389244	–29.38	NM_007662	Cadherin 15	None	Ebf1
chr8	125389246	–28.44	NM_007662	Cadherin 15	None	Ebf1
chr9	21549579	12.84	NM_026282	Ldlr	None	None
chr9	31720357	–14.51	NM_013800	Barx2	Jarid2, EZH2, Suz12	
chr9	56994574	–14.04	NM_028347	Neil1	None	None
chr9	107611227	–21.43	NM_011349	Sema3f	Mtf2, EZH2, Suz12	
chrX	11655662	–14.96	NM_029510	Bcor	Mtf2, Jarid2, EZH2, Suz12	
chrX	11658411	–23.91	NM_175046	Bcor	Mtf2, Jarid2, EZH2, Suz12	
chrX	34415040	22.79	NM_019668	Ube2a	None	None
chrX	34415077	21.67	NM_019668	Ube2a	None	None
chrX	56387270	27.18	NM_010200	Fgf13	Mtf2, EZH2	
chrX	68917537	–24.71	NM_010340	Gpr50	Mtf2, Jarid2, EZH2, Suz12	
chrX	97454071	21.48	NM_001177943	Eda	None	None
chrX	110412278	23.36	NM_033605	Dach2	None	None
chrX	130221716	30.33	NM_001105245	Pcdh19	Mtf2, Jarid2, Suz12	
chrX	158346841	–25.22	NM_198409	Nhs	None	None
chrX	160347121	27.82	NM_001290379	Ap1s2	None	None

cytosine impacts expression is still unclear. Others have also seen a lack of correlation between gene expression and treatment-related changes in methylation status [49–53]. In one study of over 230 000 cytosines, only 16.6% demonstrated a significant association between methylation and expression of a closely located TSS [54]. The association between gene body methylation and gene expression appears to be complex and context dependent [55, 56]. Even in cancerous cells with their often more robust changes in methylation, associations between gene expression and methylation are surprisingly small, and include both positive and negative correlations [57]. This may be attributed to the time-dependent sensitivity of gene expression. Alternatively, the epigenetic impact of exogenous factors such as TCE on gene expression may be indirect; via methylation-induced changes in the expression or function of some upstream regulator, and thus not obviously correlative. Alterations in methylation may only play a permissive, rather than direct, role in regulating gene expression.

Compared with the 19 autosomal chromosomes, the X chromosome had a very different profile of mean methylation levels, regardless of TCE exposure. In dramatic contrast to the autosomal chromosomes the X chromosome had very few hypomethylated CpG sites, and a much larger percentage of CpG sites with mid-range DNA methylation. Differences in X chromosome DNA methylation profiles are not surprising due to the epigenetically regulated X chromosome silencing that occurs in the blastocyst. This silencing is accomplished by a combination of epigenetic modifications involving histone deacetylation, RNA methylation, and DNA methylation [58, 59]. Comparing the methylation status of individual CpGs in the X chromosome from peripheral blood leukocytes of males and females indicated both had a set of highly methylated CpGs, while CpGs that were hypomethylated in males (under 11%) tended to be methylated in the 30–40% range in females [60]. This is largely in agreement with our analysis of the X chromosome from effector/memory CD4+ T cells of female mice. The mean

Table 2: TCE vs Control annotated immune gene expression

Symbol	REFSEQ_ID	FC	*P* value	adj. *P* value	*q*-Value	PcG	Other TF with PcG
Cytokines							
Ifit2	NM_008332.2	–2.91422	6.49E–06	0.008901	0.007645	None	Cdx1, Myod1
Tnf	NM_013693.1	–2.43709	3.44E–05	0.015926	0.01368	None	None
Ifitm3	NM_025378.2	–2.04188	0.000198	0.031075	0.026692	None	Stat5a
Amica1	NM_001005421.3	–2.01204	0.000128	0.025726	0.022097	None	None
Ifi202b	NM_008327.1	–2.00414	1.99E–06	0.005447	0.004679	None	None
Il4	NM_021283.1	–1.98215	0.00038	0.041971	0.03605	None	Nfatc2
Ifitm1	NM_026820.2	–1.86847	0.00039	0.04252	0.036523	None	None
Irf7	NM_016850.2	–1.84292	0.000657	0.054756	0.047032	None	None
Isg20	NM_020583.4	–1.75296	1.48E–05	0.011839	0.010169	None	Foxa2
Il17a	NM_010552.3	–1.68794	0.000793	0.060267	0.051766	None	Bhlhe40
Lif	NM_001039537.1	–1.50454	1.05E–05	0.01061	0.009113	None	Pax6
Il16	NM_010551	1.305869	6.96E–07	0.00394	0.003384	None	Foxa2, ATOH1
Tnfrsf26	NM_175649.5	1.346837	0.00032	0.038826	0.03335	None	Cdx1
Ing4	NM_133345.2	1.366442	0.000634	0.054238	0.046587	None	Rxra, Sox3
Traf1	NM_009421.3	1.401221	0.000837	0.062156	0.053389	None	Bhlhe40, Myod1
Ncf4	NM_008677.1	1.405497	8.09E–05	0.021965	0.018867	None	Ebf1, Myod1, Bhlhe40
Il1r2	NM_010555.4	1.459921	0.00052	0.049157	0.042223	None	Foxa2
Chemokines							
Cxcl10	NM_021274.1	–1.76465	0.000219	0.032733	0.028116	None	None
Ccrl2	NM_017466.4	–1.66005	1.25E–05	0.010725	0.009212	None	None
Cxcr4	NM_009911.2	1.634843	0.000334	0.020502	0.016849	Suz12, Jarid2, Mtf2	ATOH1
Transcription factors & enzymes							
Mycbp2	NM_207215.2	–1.64382	0.000189	0.030347	0.026066	Mtf2	Meis1, Bhlhe40, Ebf1
Trafd1	NM_172275.1	–1.58643	7.10E–05	0.021467	0.018439	None	Foxa2, Nkx2-5
Sp100	NM_013673.2	–1.31215	0.000377	0.041921	0.036008	None	Bhlhe40, Cdx1
Cxxc1	NM_028868.3	1.321214	7.64E–05	0.021965	0.018867	None	Bhlhe40
Csk	NM_007783.2	1.344270	0.0003704	0.041861	0.035956	None	Ebf1, ATOH1
Mapk11	NM_011161.4	1.341871	0.000238	0.034005	0.029208	None	Egr2, Sox3
Rap1gap	NM_001081155.1	1.344891	0.000792	0.060267	0.051766	Mtf2	Bhlhe40
Elk3	NM_205536.1	1.3791	1.47E–05	0.011839	0.010169	None	Ebf1, Stat5a
Nfkbib	NM_010908.3	1.410298	0.000119	0.025478	0.021884	None	Foxa2
Rag1ap1	NM_009057.2	1.42048	0.000158	0.027165	0.023333	None	Ebf1
Mt1	NM_013602.2	2.12539	7.29E–06	0.009447	0.008114	None	None
Cell cycle							
Gadd45g	NM_011817.1	–1.30109	7.79E–05	0.021965	0.018867	Suz12, Mtf2	ATOH1
Cdc23	NM_178347	1.340161	5.13E–06	0.0083	0.007129	None	Foxa2
Apoptosis							
Daxx	NM_007829.3	–1.79108	3.82E–05	0.016024	0.013764	None	None
Fasl	NM_010177.3	–1.45356	0.000115	0.025294	0.021726	None	Cdx1
Bcl11b	NM_021399.2	1.311508	0.000262	0.035376	0.030386	EZH2, Suz12, Jarid2, Mtf2	
Pdcd2	NM_008799.2	1.356754	3.22E–06	0.006902	0.005928	None	Bhlhe40, Meis1
Pdcd4	NM_011050.3	1.407455	0.000546	0.05012	0.04305	None	Foxa2, Myod1
Integrins							
Sdc3	NM_011520.3	–1.84389	0.000208	0.031629	0.027168	None	Hoxc9, Sox3
Ly6c1	NM_010741.2	–1.50191	0.000146	0.026013	0.022343	None	Cdx1, Bhlhe40
Cd247	NM_031162.1	1.300788	0.000203	0.031216	0.026812	None	Foxa2, Creg1, Tal1
Leng9	NM_175529.3	1.303316	0.000444	0.045017	0.038667	Mtf2	None
Mic2l1	NM_138309.1	1.33617	9.20E–05	0.022878	0.019651	None	Stat5a
Hist1h2ai	NM_178182.1	1.419197	0.000898	0.063308	0.054378	None	None
Hist1h1c	NM_015786.1	1.592885	0.000622	0.054158	0.046519	None	Cdx1, Bhlhe40
Ctla4	NM_009843.3	1.472701	0.000221	0.03284	0.028208	None	None
Miscellaneous							
Birc2	NM_007465.1	1.372856	1.75E–05	0.012794	0.010989	None	Rxra, Cdx1
Ddb2	NM_028119.4	1.37404	1.22E–05	0.010725	0.009212	None	Cdx1, Rxra, Tal1
Rfx1	NM_009055.2	1.519909	0.000101	0.023946	0.020568	None	Myod1

methylation distribution observed in the X chromosome does not reflect averaging of two chromosomes, one of which was completely hypermethylated. Instead, the profile indicates the presence of a more complex methylation pattern. It remains to be determined whether this pattern is due to the DNA methylation on the inactivated X chromosome, the active X chromosome, or a combination of both.

One surprising result was the apparent connection between TCE-altered CpGs and PcG protein binding regions. PcG proteins were first identified as regulators of embryonic development

and stem cell pluripotency [61]. PcG proteins form two complexes in mammals; polycomb-repressive complex 1 (PRC1) and PRC2. PRC2 mediates H3K27me3, which is thought to inhibit transcription by a mechanism involving H2A ubiquitination and/or chromatin compaction [62, 63]. The initial work on PcG proteins conducted in embryonic stem cells identified a complex interaction between PRC2 binding and DNA methylation. Although the majority of CpG islands do not normally recruit PcG proteins, there is an anomalous conservation of CpG sites at PRC2-binding domains [64, 65]. This connection seems to involve a certain level of reciprocal regulation. For example, PRC2 binding represses DNA methylation at the PRC2 target regions in embryonic stem cells [66]. Similarly, DNA methylation appears to regulate PRC2 binding. A high density of unmethylated CpG sites reportedly promotes PcG protein binding [67]. Removal of DNA methylation promotes the accumulation of the PRC2 complex in inappropriate genomic loci, indicating that DNA methylation is capable of attenuating PRC2 binding [68]. However, there is evidence in somatic cells and cancer cells that DNA methylation and PRC2 binding may not be mutually exclusive, and may in fact work together to suppress specific gene expression [65].

The role of PcG proteins in the regulation of immune function specifically is still being defined. Late stages of human B cell differentiation showed methylation gain at PcG-repressed areas, thus suggesting a need for DNA methylation to block PcG protein binding in non-transformed lymphocytes [69]. In terms of T cells, PcG proteins have been shown to form a complex with the Ikaros transcription factor to regulate thymocyte development [70]. They can also regulate the function of mature peripheral T cells [71]. For example, EZH2, a component of PRC2, has recently been shown by others to be highly expressed in $CD4^+$ T cells [72], where it reportedly associates with Foxp3 to mediate gene repression and suppressive function [73]. Loss of EZH2 *in vivo* caused increase immune pathology, including colitis, in part due to a lack of functional Treg cells [73, 74]. EZH2 also controls differentiation and plasticity of $CD4^+$ Th1 and Th2 cells by binding and controlling expression of Tbx21 and Gata3 [75]. Deletion of EZH2 leads to increased generation of effector/memory $CD4^+$ T cells with an increased production of effector cytokines including IFN-γ [73]. Cell differentiation is accompanied by losses and gains of H3K27me3 at many promoters at many stages of the process, while DNA methylation is altered at only a relatively small number of promoters during differentiation. This suggests that PcG protein binding represents a more robust suppression than DNA methylation.

There were some limitations associated with the current study. RRBS analysis does not distinguish between 5-methylcytosine (5mC) and 5-hydroxymethylcytosine (5hmC). The ten-eleven translocation (TET) family of proteins can oxidize 5mC to 5hmC, a mark not effectively maintained by Dnmt1, thus leading to demethylation as cells divide. Polarization of $CD4^+$ T cells toward Th1 and Th2 lineages is accompanied by changes in 5hmc-mediated DNA de-methylation of key genes [76], and defects in DNA hydroxymethylation have been demonstrated in both thymocytes and peripheral $CD4^+$ T cells from patients with autoimmune diseases [77, 78]. A direct correlation between levels of 5hmc and H3K27me has been described in a variety of somatic tissues [79]. It will be important to distinguish whether the enrichment of PcG protein binding sites in the current study are associated with TCE-induced alterations DNA methylation or DNA hydroxymethylation.

Despite its limitations, the current study has demonstrated effects of TCE on genome-wide and gene-specific DNA methylation. This included a TCE-induced decrease in methylation variance, and the observation that TCE-induced changes in CpG methylation tended to occur in regulatory elements that bound suppressive PcG proteins. These effects may be mechanistically important since many autoimmune diseases are driven by effector/memory $CD4^+$ T cells which are resistant to several mechanisms designed to guard against the expansion of autoreactive $CD4^+$ T cells. Thus, any epigenetic mechanism that targeted effector/memory $CD4^+$ T cells could have important functional consequences. Activation and subsequent gene expression in $CD4^+$ T cells is a complex process. Aside from epigenetic mechanisms such as DNA methylation and histone acetylation, this process is also regulated by the levels and/or phosphorylation state of transcription factors and other signaling molecules. Understanding the contribution of all these factors toward $CD4^+$ T cell activation is going to require complex modeling. The epigenetic alteration of polycomb protein binding may be another component in this process. The possibility that TCE alters DNA methylation in PcG protein binding sites, suggests that an associated alteration in PRC2 binding, and downstream upregulation of proinflammatory Th1 cytokines could play a role in the ability of TCE to promote autoimmunity.

Acknowledgments

We thank Dr Damir Herman for initial coaching on the RRBS method, Dr Kartik Shankar for recommendations on RRBS sample preparation, and Dr Stewart Macleod for helpful advice on next generation sequencing, and for performing the Illumina sequencing.

Data Availability

Data are available in the Supplementary Material.

Funding

This work was supported by grants from the Arkansas Biosciences Institute, the National Institutes of Health (R01ES021484), and the UAMS Translational Research Institute (National Institutes of Health UL1RR029884).

Supplementary Data

Supplementary data is available at *EnvEpig* online.

Conflict of interest statement. None declared.

References

1. Kawakami N, Odoardi F, Ziemssen T, Bradl M, Ritter T, Neuhaus O, Lassmann H, Wekerle H, Flugel A. Autoimmune CD4+ T cell memory: lifelong persistence of encephalitogenic T cell clones in healthy immune repertoires. *J Immunol* 2005; **175**:69–81.
2. Oling V, Reijonen H, Simell O, Knip M, Ilonen J. Autoantigen-specific memory CD4+ T cells are prevalent early in progression to Type 1 diabetes. *Cell Immunol* 2012;**273**:133–9.
3. Elyaman W, Kivisakk P, Reddy J, Chitnis T, Raddassi K, Imitola J, Bradshaw E, Kuchroo VK, Yagita H, Sayegh MH, et al. Distinct functions of autoreactive memory and effector CD4+ T cells in experimental autoimmune encephalomyelitis. *Am J Pathol* 2008;**173**:411–22.

4. Williams JL, Kithcart AP, Smith KM, Shawler T, Cox GM, Whitacre CC. Memory cells specific for myelin oligodendrocyte glycoprotein (MOG) govern the transfer of experimental autoimmune encephalomyelitis. *J Neuroimmunol* 2011;**234**: 84–92.
5. ATSDR: Toxicological Profile for Trichloroethylene, US Department of Health and Human Services, Agency for Toxic Substances and Disease Registry 2014.
6. Gilbert KM, Blossom SJ, Erickson SW, Reisfeld B, Zurlinden TJ, Broadfoot B, West K, Bai S, Cooney CA. Chronic exposure to water pollutant trichloroethylene increased epigenetic drift in $CD4^+$ T cells. *Epigenomics* 2016;**8**:633–49.
7. Byers VS, Levin AS, Ozonoff DM, Baldwin RW. Association between clinical symptoms and lymphocyte abnormalities in a population with chronic domestic exposure to industrial solvent-contaminated domestic water supply and a high incidence of leukemia. *Cancer Immunol Immunother* 1988;**27**:77–82.
8. Yanez DS, Moran M, Unamuno P, Armijo M. Silica and trichloroethylene-induced progressive systemic sclerosis. *Dermatol* 1992;**184**:98–102.
9. Hansen BL, Isager H. A scleroderma-resembling disease-exposure to trichloroethylene and trichloroethane, is there a causal connection? *Ugeskr Laeger* 1988;**150**:805–8.
10. Saihan EM, Burton JL, Heaton KW. A new syndrome with pigmentation, scleroderma, gynaecomastia, Raynaud's phenomenon and peripheral neuropathy. *Br J Dermatol* 1978;**99**:437–40.
11. Flindt-Hansen H, Isager H. Scleroderma after occupational exposure to trichloroethylene and trichlorethane. *Toxicol Lett* 1987;**95**:173–81.
12. Czirjak L, Pocs E, Szegedi G. Localized scleroderma after exposure to organic solvents. *Dermatology (Basel)* 1994;**189**:399–401.
13. Lockey JE, Kelly CR, Cannon GW, Colby TV, Aldrich V, Livingston GK. Progressive systemic sclerosis associated with exposure to trichloroethylene. *J Occup Med* 1997;**29**:493–6.
14. Dubrow R, Gute DM. Cause-specific mortality among Rhode Island jewelry workers. *Am J Ind Med* 1987;**12**:579–93.
15. Gist GL, Burg JR. Trichloroethylene – a review of the literature from a health effects perspective. *Toxicol Ind Health* 1995;**11**: 253–307.
16. Kilburn KH, Washaw RW. Prevalence of symptoms of systemic lupus erythematosus (SLE) and of fluorescent antinuclear antibodies associated with chronic exposure to trichloroethylene and other chemicals in well water. *Environ Res* 1992;**57**:1–9.
17. Clark LC, Giulano A, Walsh B, Guernsey de Zaplen J, Alberts DS, Meister J, Manson TS, *The Santa Cruz County Community Health Survey*. Phoenix, AZ: Arizona Department of Health Services, 1994.
18. Nietert PJ, Sutherland SE, Silver RM, Pandey JP, Knapp RG, Hoel DG, Dosemeci M. Is occupational organic solvent exposure a risk factor for scleroderma? *Arthritis Rheum* 1998;**41**:1111–9.
19. Iavicoli I, Marinaccio A, Carelli G. Effects of occupational trichloroethylene exposure on cytokine levels in workers. *J Occup Environ Med* 2005;**47**:453–7.
20. Yi J, Teng YX, Zang D, Zhou W, Dong HY, Niu Y, Bin P, Huang XQ, Zheng YX, Dai YF. Analysis of subgroups of lymphocyte in peripheral blood among dermatitis medicamentosa-like of trichloroethylene patients and healthy exposed workers. *Zhonghua Yu Fang Yi Xue Za Zhi* 2011;**45**:1017–21.
21. Gilbert KM, Przybyla B, Pumford NR, Han T, Fuscoe J, Schnackenberg LK, Holland RD, Doss JC, MacMillan-Crow LA, Blossom SJ. Delineating liver events in trichloroethylene-induced autoimmune hepatitis. *Chem Res Toxicol* 2009;**22**: 626–32.
22. Griffin JM, Blossom SJ, Jackson SK, Gilbert KM, Pumford NR. Trichloroethylene accelerates an autoimmune response in association with Th1 T cell activation in MRL+/+ mice. *Immunopharmacology* 2000;**46**:123–37.
23. Wang G, Wang J, Ma H, Ansari GA, Khan MF. N-Acetylcysteine protects against trichloroethene-mediated autoimmunity by attenuating oxidative stress. *Toxicol Appl Pharmacol* 2013;**273**: 189–95.
24. Komori HK, Hart T, LaMere SA, Chew PV, Salomon DR. Defining CD4 T cell memory by the epigenetic landscape of CpG DNA methylation. *J Immunol* 2015;**194**:1565–79.
25. Hashimoto S, Ogoshi K, Sasaki A, Abe J, Qu W, Nakatani Y, Ahsan B, Oshima K, Shand FH, Ametani A, et al. Coordinated changes in DNA methylation in antigen-specific memory CD4 T cells. *J Immunol* 2013;**190**:4076–91.
26. Lleo A, Zhang W, Zhao M, Tan Y, Bernuzzi F, Zhu B, Liu Q, Tan Q, Malinverno F, Valenti L, et al. DNA methylation profiling of the X chromosome reveals an aberrant demethylation on CXCR3 promoter in primary biliary cirrhosis. *Clin Epigenetics* 2015;**7**:61–0098.
27. Altorok N, Coit P, Hughes T, Koelsch KA, Stone DU, Rasmussen A, Radfar L, Scofield RH, Sivils KL, Farris AD, et al. Genome-wide DNA methylation patterns in naive CD4+ T cells from patients with primary Sjogren's syndrome. *Arthritis Rheumatol* 2014;**66**:731–9.
28. Meyer B, Chavez RA, Munro JE, Chiaroni-Clarke RC, Akikusa JD, Allen RC, Craig JM, Ponsonby AL, Saffery R, Ellis JA. DNA methylation at IL32 in juvenile idiopathic arthritis. *Sci Rep* 2015;**5**:11063.
29. Wang Y, Shu Y, Xiao Y, Wang Q, Kanekura T, Li Y, Wang J, Zhao M, Lu Q, Xiao R. Hypomethylation and overexpression of ITGAL (CD11a) in CD4(+) T cells in systemic sclerosis. *Clin Epigenetics* 2014;**6**:25–6.
30. Wu Z, Mei X, Zhao D, Sun Y, Song J, Pan W, Shi W. DNA methylation modulates HERV-E expression in CD4+ T cells from systemic lupus erythematosus patients. *J Dermatol Sci* 2015; **77**:110–6.
31. Coit P, Renauer P, Jeffries MA, Merrill JT, McCune WJ, Maksimowicz-McKinnon K, Sawalha AH. Renal involvement in lupus is characterized by unique DNA methylation changes in naive CD4+ T cells. *J Autoimmun* 2015;**61**:29–35.
32. Zhang Y, Zhao M, Sawalha AH, Richardson B, Lu Q. Impaired DNA methylation and its mechanisms in CD4(+)T cells of systemic lupus erythematosus. *J Autoimmun* 2013;**41**:92–9.
33. Quddus J, Johnson KJ, Gavalchin J, Amento EP, Chrisp CE, Yung RL, Richardson BC. Treating activated CD4+ T cells with either of two distinct DNA methyltransferase inhibitors, 5-azacytidine or procainamide, is sufficient to cause a lupus-like disease in syngeneic mice. *J Clin Invest* 1993;**92**:38–53.
34. Yung RL, Quddus J, Chrisp CE, Johnson KJ, Richardson BC. Mechanism of drug-induced lupus. I. Cloned Th2 cells modified with DNA methylation inhibitors in vitro cause autoimmunity in vivo. *J Immunol* 1995;**154**:3025–35.
35. Ivanova EA, Orekhov AN. T helper lymphocyte subsets and plasticity in autoimmunity and cancer: an overview. *Biomed Res Int* 2015;**2015**:327470.
36. Hirahara K, Nakayama T. CD4+ T-cell subsets in inflammatory diseases: beyond the Th1/Th2 paradigm. *Int Immunol* 2016;**28**:163–71.
37. Cosmi L, Maggi L, Santarlasci V, Liotta F, Annunziato F. T helper cells plasticity in inflammation. *Cytometry A* 2014;**85**: 36–42.
38. Gilbert KM, Nelson AR, Cooney CA, Reisfeld B, Blossom SJ. Epigenetic alterations may regulate temporary reversal of

CD4(+) T cell activation caused by trichloroethylene exposure. *Toxicol Sci* 2012;**127**:169–78.
39. Gilbert KM, Blossom SJ, Erickson SW, Broadfoot B, West K, Bai S, Li J, Cooney CA. Chronic exposure to trichloroethylene increases DNA methylation of the Ifng promoter in CD4+ T cells. *Toxicol Lett* 2016;**260**:1–7.
40. Gu H, Smith ZD, Bock C, Boyle P, Gnirke A, Meissner A. Preparation of reduced representation bisulfite sequencing libraries for genome-scale DNA methylation profiling. *Nat Protoc* 2011;**6**:468–81.
41. Gilbert KM, Pumford NR, Blossom SJ. Environmental contaminant trichloroethylene promotes autoimmune disease and inhibits T-cell apoptosis in MRL+/+ mice. *J Immunotox* 2006;**3**: 263–7.
42. Boyle P, Clement K, Gu H, Smith ZD, Ziller M, Fostel JL, Holmes L, Meldrim J, Kelley F, Gnirke A, et al. Gel-free multiplexed reduced representation bisulfite sequencing for large-scale DNA methylation profiling. *Genome Biol* 2012;**13**: R92–13.
43. Akalin A, Kormaksson M, Li S, Garrett-Bakelman FE, Figueroa ME, Melnick A, Mason CE. methylKit: a comprehensive R package for the analysis of genome-wide DNA methylation profiles. *Genome Biol* 2012;**13**:R87–13.
44. Lee JH, Park SJ, Kenta N. An integrative approach for efficient analysis of whole genome bisulfite sequencing data. *BMC Genomics* 2015;**16(Suppl. 12)**:S14.
45. Ziller MJ, Stamenova EK, Gu H, Gnirke A, Meissner A. Targeted bisulfite sequencing of the dynamic DNA methylome. *Epigenetics Chromatin* 2016;**9**:55.
46. Ambler G, Royston P. Fractional polynomial model selection procedures: investigation of Type I error rate. *J Stat Simul Comput* 2001;**69**:89–108.
47. Elliott G, Hong C, Xing X, Zhou X, Li D, Coarfa C, Bell RJ, Maire CL, Ligon KL, Sigaroudinia M, et al. Intermediate DNA methylation is a conserved signature of genome regulation. *Nat Commun* 2015;**6**:6363.
48. Jacoby M, Gohrbandt S, Clausse V, Brons NH, Muller CP. Interindividual variability and co-regulation of DNA methylation differ among blood cell populations. *Epigenetics* 2012;**7**: 1421–34.
49. Kaneko KJ, Rein T, Guo ZS, Latham K, DePamphilis ML. DNA methylation may restrict but does not determine differential gene expression at the Sgy/Tead2 locus during mouse development. *Mol Cell Biol* 2004;**24**:1968–82.
50. Moarii M, Boeva V, Vert JP, Reyal F. Changes in correlation between promoter methylation and gene expression in cancer. *BMC Genomics* 2015;**16**:873–1994.
51. Bendall ML, Luong K, Wetmore KM, Blow M, Korlach J, Deutschbauer A, Malmstrom RR. Exploring the roles of DNA methylation in the metal-reducing bacterium Shewanella oneidensis MR-1. *J Bacteriol* 2013;**195**:4966–74.
52. Willems E, Guerrero-Bosagna C, Decuypere E, Janssens S, Buyse J, Buys N, Jensen P, Everaert N. Differential expression of genes and DNA methylation associated with prenatal protein undernutrition by albumen removal in an avian model. *Sci Rep* 2016;**6**:20837.
53. Bysani M, Perfilyev A, de Mello VD, Ronn T, Nilsson E, Pihlajamaki J, Ling C. Epigenetic alterations in blood mirror age-associated DNA methylation and gene expression changes in human liver. *Epigenomics* 2017;**9**:105–22.
54. Medvedeva YA, Khamis AM, Kulakovskiy IV, Ba-Alawi W, Bhuyan MS, Kawaji H, Lassmann T, Harbers M, Forrest AR, Bajic VB. Effects of cytosine methylation on transcription factor binding sites. *BMC Genomics* 2014;**15**:119–5.
55. Varley KE, Gertz J, Bowling KM, Parker SL, Reddy TE, Pauli-Behn F, Cross MK, Williams BA, Stamatoyannopoulos JA, Crawford GE, et al. Dynamic DNA methylation across diverse human cell lines and tissues. *Genome Res* 2013;**23**:555–67.
56. Ehrlich M, Lacey M. DNA methylation and differentiation: silencing, upregulation and modulation of gene expression. *Epigenomics* 2013;**5**:553–68.
57. Long MD, Smiraglia DJ, Campbell MJ. The genomic impact of DNA CpG methylation on gene expression; relationships in prostate cancer. *Biomolecules* 2017;**7**:E15.
58. Pinheiro I, Heard E. X chromosome inactivation: new players in the initiation of gene silencing. *F1000Res* 2017;**6**:1–10.
59. Balaton BP, Cotton AM, Brown CJ. Derivation of consensus inactivation status for X-linked genes from genome-wide studies. *Biol Sex Differ* 2015;**6**:35.
60. Cotton AM, Price EM, Jones MJ, Balaton BP, Kobor MS, Brown CJ. Landscape of DNA methylation on the X chromosome reflects CpG density, functional chromatin state and X-chromosome inactivation. *Hum Mol Genet* 2015;**24**:1528–39.
61. Khan AA, Lee AJ, Roh TY. Polycomb group protein-mediated histone modifications during cell differentiation. *Epigenomics* 2015;**7**:75–84.
62. Eskeland R, Freyer E, Leeb M, Wutz A, Bickmore WA. Histone acetylation and the maintenance of chromatin compaction by Polycomb repressive complexes. *Cold Spring Harb Symp Quant Biol* 2010;**75**:71–8.
63. Stock JK, Giadrossi S, Casanova M, Brookes E, Vidal M, Koseki H, Brockdorff N, Fisher AG, Pombo A. Ring1-mediated ubiquitination of H2A restrains poised RNA polymerase II at bivalent genes in mouse ES cells. *Nat Cell Biol* 2007;**9**:1428–35.
64. Tanay A, O'Donnell AH, Damelin M, Bestor TH. Hyperconserved CpG domains underlie Polycomb-binding sites. *Proc Natl Acad Sci U S A* 2007;**104**:5521–6.
65. McCabe MT, Lee EK, Vertino PM. A multifactorial signature of DNA sequence and polycomb binding predicts aberrant CpG island methylation. *Cancer Res* 2009;**69**:282–91.
66. Thornton SR, Butty VL, Levine SS, Boyer LA. Polycomb Repressive Complex 2 regulates lineage fidelity during embryonic stem cell differentiation. *PLoS ONE* 2014;**9**:e110498.
67. Lynch MD, Smith AJ, De GM, Flenley M, Hughes JR, Vernimmen D, Ayyub H, Sharpe JA, Sloane-Stanley JA, Sutherland L, et al. An interspecies analysis reveals a key role for unmethylated CpG dinucleotides in vertebrate Polycomb complex recruitment. *EMBO J* 2012;**31**:317–29.
68. Brinkman AB, Gu H, Bartels SJ, Zhang Y, Matarese F, Simmer F, Marks H, Bock C, Gnirke A, Meissner A, et al. Sequential ChIP-bisulfite sequencing enables direct genome-scale investigation of chromatin and DNA methylation cross-talk. *Genome Res* 2012;**22**:1128–38.
69. Kulis M, Merkel A, Heath S, Queiros AC, Schuyler RP, Castellano G, Beekman R, Raineri E, Esteve A, Clot G, et al. Whole-genome fingerprint of the DNA methylome during human B cell differentiation. *Nat Genet* 2015;**47**:746–56.
70. Oravecz A, Apostolov A, Polak K, Jost B, Le GS, Chan S, Kastner P. Ikaros mediates gene silencing in T cells through Polycomb repressive complex 2. *Nat Commun* 2015;**6**:8823.
71. Zhang Y, Kinkel S, Maksimovic J, Bandala-Sanchez E, Tanzer MC, Naselli G, Zhang JG, Zhan Y, Lew AM, Silke J, et al. The polycomb repressive complex 2 governs life and death of peripheral T cells. *Blood* 2014;**124**:737–49.
72. Onodera A, Tumes DJ, Watanabe Y, Hirahara K, Kaneda A, Sugiyama F, Suzuki Y, Nakayama T. Spatial interplay between polycomb and trithorax complexes controls transcriptional activity in T lymphocytes. *Mol Cell Biol* 2015;**35**:3841–53.

73. Yang XP, Jiang K, Hirahara K, Vahedi G, Afzali B, Sciume G, Bonelli M, Sun HW, Jankovic D, Kanno Y, et al. EZH2 is crucial for both differentiation of regulatory T cells and T effector cell expansion. *Sci Rep* 2015;**5**:10643.
74. Sarmento O, Xiong Y, Sun Z, Svingen P, Bamidele A, Smyrk T, Nair A, Baheti S, McGovern D, Friton J, et al. O-015 YI alterations in the FOXP3-EZH2 pathway associates with increased susceptibility to colitis in both mice and human. *Inflamm Bowel Dis* 2016;**22(Suppl. 1)**:S5–6.
75. Tumes DJ, Onodera A, Suzuki A, Shinoda K, Endo Y, Iwamura C, Hosokawa H, Koseki H, Tokoyoda K, Suzuki Y, et al. The polycomb protein Ezh2 regulates differentiation and plasticity of CD4(+) T helper type 1 and type 2 cells. *Immunity* 2013; **39**:819–32.
76. Nestor CE, Lentini A, Hagg NC, Gawel DR, Gustafsson M, Mattson L, Wang H, Rundquist O, Meehan RR, Klocke B, et al. 5-Hydroxymethylcytosine remodeling precedes lineage specification during differentiation of human CD4(+) T cells. *Cell Rep* 2016;**16**:559–70.
77. Zhao M, Wang J, Liao W, Li D, Li M, Wu H, Zhang Y, Gershwin Me, Lu Q. Increased 5-hydroxymethylcytosine in CD4(+) T cells in systemic lupus erythematosus. *J Autoimmun* 2016;**69**:64–73.
78. Liu T, Sun J, Wang Z, Yang W, Zhang H, Fan C, Shan Z, Teng W. Changes in the DNA methylation and hydroxymethylation status of the intercellular adhesion molecule 1 gene promoter in thyrocytes from autoimmune thyroiditis patients. *Thyroid* 2017;**27**:838–45.
79. Haffner MC, Pellakuru LG, Ghosh S, Lotan TL, Nelson WG, De Marzo AM, Yegnasubramanian S. Tight correlation of 5-hydroxymethylcytosine and Polycomb marks in health and disease. *Cell Cycle* 2013;**12**:1835–41.